Adsorption and Reaction of SO 2 with a Polycrystalline UO 2 Film: Promotion of S–O Bond Cleavage by Creation of O-Defects and Na or Ca Coadsorption

5 AUTHORS, INCLUDING:

M. N. Hedhili

King Abdullah University of Science and Tech…

81 PUBLICATIONS 943 CITATIONS

SEE PROFILE

T. Gouder

European Commission

100 PUBLICATIONS 1,139 CITATIONS

SEE PROFILE

Adsorption and Reaction of SO$_2$ with a Polycrystalline UO$_2$ Film: Promotion of S−O Bond Cleavage by Creation of O-Defects and Na or Ca Coadsorption

T. W. Schlereth,[†] M. N. Hedhili,[†,‡] B. V. Yakshinskiy,[†] T. Gouder,[§] and T. E. Madey*,[†]

Laboratory for Surface Modification, Department of Physics and Astronomy, Rutgers, The State University of New Jersey, Piscataway, New Jersey 08854, and European Commission, Joint Research Center, Institute for Transuranium Elements, Postfach 2340, D-76125 Karlsruhe, Germany

To characterize UO$_2$ for its possible use in desulfurization applications, the interactions of molecular sulfur dioxide (SO$_2$) with a polycrystalline uranium dioxide film have been studied by means of X-ray photoelectron spectroscopy (XPS), temperature-programmed desorption (TPD), and low-energy ion scattering (LEIS). The stoichiometric, oxygen-deficient, calcium-precovered and sodium-precovered UO$_2$ surfaces have been characterized. The changes in oxide reactivity upon creation of oxygen vacancies and coadsorption of sodium and calcium have been studied. After creation of a reduced UO$_{2-x}$ surface ($x \sim 0.44$) via Ar$^+$ sputtering, the U 4f XPS spectrum shows conspicuous differences that are good indicators of the surface stoichiometry. Molecular SO$_x$ formation ($x = 2-4$) is observed after SO$_2$ deposition onto stoichiometric UO$_2$ and onto UO$_2$ precovered with small amounts (<1 ML) of Na or Ca; complete dissociation of SO$_2$ is not observed. Heating leads to desorption of the SO$_x$ species and to transformation of SO$_2$ to SO$_3$ and SO$_3$ to SO$_4$. On oxygen-deficient UO$_2$ and on UO$_2$ precovered with large Na or Ca coverages (≥ 4 ML), both the formation of SO$_x$ species and complete dissociation of SO$_2$ are observed. A higher thermal stability of the sulfur components is observed on these surfaces. In all cases for which dissociation occurs, the XPS peak of atomic sulfur shows similar structure: three different binding states are observed. The reactivity of oxygen-deficient UO$_2$ and sodium- and calcium-precovered UO$_2$ (coverages ≥ 4 ML) is attributed to charge transfer into the antibonding LUMO of the adsorbed molecule.

1. Introduction

Metal oxides have a large number of applications, including the development of corrosion protection, solid-state gas sensors, and fuel cell electrodes, as well as microelectronics and heterogeneous catalysis. Recently, interest in exploring the physical, electronic, and catalytic properties of uranium dioxide (UO$_2$) has increased. The reason for this is the desire to find possible applications for depleted uranium, which is currently stored in huge stockpiles in the United States and elsewhere.[1,2] Depleted uranium has a reduced concentration of the fissionable isotope U-235; it is a waste product of nuclear fuel production. Various possible utilizations, such as the use of uranium oxide as semiconductor material, catalyst, or even radiation shielding are being explored.[1,3] Uranium oxides show catalytic activity for the destruction of volatile organic compounds (VOC) such as butane, benzene, and chlorobenzene.[4,5] Uranium dioxide has also been used as a catalytic support for steam reforming of methane.[6] Motivated by the fact that thousands of metric tons of uranium fuel are placed in water storage, the interaction of water with UO$_2$(001),[7] UO$_2$(100),[8] and UO$_2$(111)[9] has been studied. Also the influence of surface defects on the reactions of ethanol and carboxylic acids with UO$_2$(111) has been investigated.[10,11] To probe the possible use of UO$_2$ as a catalyst in hydrodesulfurization reactions (HDS), the adsorption of H$_2$S

onto UO$_2$(001)[12] and polycrystalline UO$_2$,[13] as well as the interactions of thiophene with stoichiometric and O-deficient polycrystalline UO$_2$,[14] has been examined.

Sulfur dioxide formed during the combustion of fossil fuels is a major air pollutant that causes health risks, environmental hazards, and equipment corrosion.[15] In industrial applications SO$_2$ is known to poison metal/oxide catalysts. To reduce these negative effects SO$_2$ has to be removed from effluent gases. At present, the most widely used technique is scrubbing, in which solid compounds such as CaCO$_3$ (limestone) are employed to remove SO$_2$ via a chemical reaction.[15] In another method, the SO$_2$-containing stream is passed over a high area metal oxide bed (CaO, BaO, MgO, ZnO, TiO$_2$, etc.) and the molecules are trapped as SO$_x$ species.[16] All these techniques result in huge amounts of solid waste that require disposal in landfills. Thus, there is a need for new technologies to reduce the amount of waste generated during the removal of SO$_2$. There is a general desire to employ metal oxides as catalysts for the destruction of SO$_2$ (the DeSO$_x$ process) via the Claus reaction SO$_2$ + 2H$_2$S → 2H$_2$O + 3S$_{solid}$ or via the reaction SO$_2$ + 2CO → 2CO$_2$ + S$_{solid}$.[16] Metal oxides, such as NiO,[17] CeO$_2$,[18] MoO$_2$,[19,20] ZnO,[19,21] and MgO,[16,22] have been extensively examined for their activity toward the destruction of SO$_2$. Many of these oxides are able to oxidize SO$_2$ forming SO$_x$ ($x = 3, 4$) species, but only on MoO$_2$ dissociation of small amounts of SO$_2$ is observed. Catalytic dissociation of SO$_2$ using CeO$_2$ and Ca-doped CeO$_2$ as catalysts in a gas stream reactor has been reported.[23,24] There are no published reports for the interaction of SO$_2$ with UO$_2$. The research is motivated by the possibility of using UO$_2$ as a catalyst for the destruction of SO$_2$.

* Corresponding author. Tel.: +1-732-445-5185. Fax: +1-732-445-4991. E-mail address: madey@physics.rutgers.edu.
† Rutgers, The State University of New Jersey.
‡ Permanent address: Laboratoire de Physique de la Matière Condensée, Faculté des Sciences de Tunis, 1060 Tunis, Tunisia.
§ Institute for Transuranium Elements.

In this paper the interactions of sulfur dioxide with uranium dioxide are studied by means of X-ray photoelectron spectroscopy (XPS), temperature-programmed desorption (TPD), and low-energy ion scattering (LEIS).

2. Experimental Section

All experiments were carried out under UHV conditions in a chamber with base pressure of $\sim 5 \times 10^{-11}$ Torr. The chamber is equipped with XPS, TPD, and LEIS. A detailed description of the experimental apparatus has been given previously.[12,13] The sample is mounted onto an $x-y-z$ rotary manipulator, which allows cooling to ~ 100 K by liquid nitrogen and resistive heating to $T > 600$ K. The polycrystalline ~ 1000 Å thick UO_2 film was prepared in Karlsruhe by reactive sputtering of uranium onto a molybdenum substrate ($10 \times 10 \times 1$ mm^3) under oxygen atmosphere. The molybdenum plate is mounted via Ta support wires, which allow for resistive heating of the sample. For temperature measurements, a chromel/alumel thermocouple is spot-welded onto the edge of the sample.

Research grade SO_2 (Matheson) with a purity of 99.98% is dosed onto the sample through a capillary array gas doser, which provides a flux enhancement of ~ 50 times compared to dosing via backfilling. The purity is analyzed with a quadrupole mass spectrometer prior to use. Sodium is deposited from a SAES Getter source, whereas calcium deposition is performed using a specially built metal evaporator.[25] All XPS spectra are recorded using Al Kα excitation and grazing takeoff angle (70° with respect to sample normal), with the analyzer operating mode FAT 22 (fixed analyzer transmission at a pass energy of 22 eV). The spectra are calibrated using the binding energy of the U $4f_{7/2}$ peak of stoichiometric UO_2 (~ 280.1 eV). The sample is typically cleaned by sputtering with Ar$^+$ ions (1.5 keV, 1 μA), followed by annealing to 500 K in the presence of oxygen (5×10^{-7} Torr) for 5 min to restore stoichiometry. The cleanliness and stoichiometry of the sample are monitored by XPS and LEIS. Oxygen defects are created by Ar$^+$ sputtering (1.5 keV) of the clean, reoxidized sample for 20 min at a sample current of ~ 1.5 μA.

3. Results

3.1. Adsorption and Desorption of SO_2 on Stoichiometric UO_2.
Figure 1 displays a series of TPD spectra for SO_2 (64 amu) adsorbed on stoichiometric UO_2 at 100 K as a function of increasing exposure. Reported exposures are uncorrected for the doser enhancement factor of ~ 50; the heating rate is 2.5 K/s. The inset shows the spectra for small exposures (≤ 0.018 L) of SO_2. For a very small dose of SO_2 ($\sim 3 \times 10^{-4}$ L), a broad desorption peak with peak maximum as high as 495 K is found. The desorption peak shifts to lower temperatures with increasing SO_2 exposures.

A relatively sharp peak centered at ~ 133 K appears and continues to grow in intensity (does not saturate); such behavior is consistent with desorption from a physisorbed multilayer of SO_2. On the basis of the appearance and growth of the multilayer peak and the saturation of the high-temperature feature, we identify an exposure of 0.018 L with the formation of $\sim 80\%$ of a monolayer. The increased background above ~ 550 K for higher coverages is associated with desorption from the sample holder. Taking this background into account, we measure a maximum desorption temperature of ~ 550 K (i.e. no desorption occurs for $T > 550$ K). For a multilayer of SO_2 similar desorption peak temperature values (~ 133 K) are reported for various metal surfaces[26-30] and Au supported on MgO(100).[31] The estimated desorption energy for multilayer SO_2, according
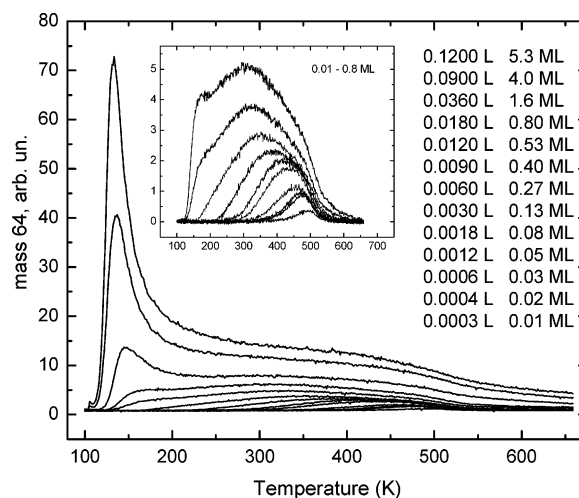

Figure 1. TPD spectra (64 amu SO_2^+ signal) for different amounts of SO_2 adsorbed on stoichiometric UO_2 at 100 K. The linear heating rate was ~ 2.5 K/s. The inset shows the spectra for small coverages of SO_2. The high background signal manifest above ~ 550 K for higher coverages can be explained by desorption from the sample holder.
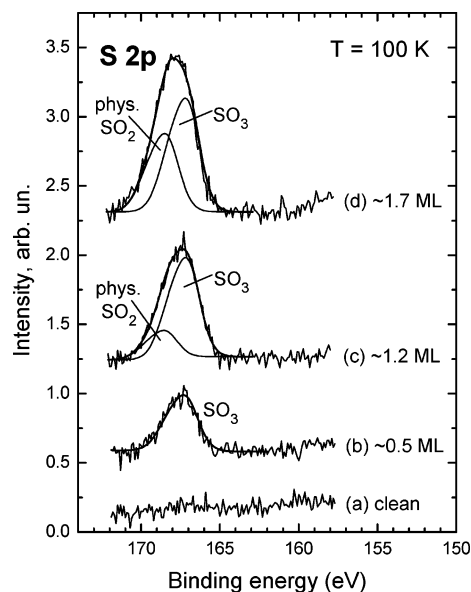

Figure 2. S 2p grazing angle XPS spectra for different doses of SO_2 on polycrystalline UO_2 at 100 K. For each spectrum a new SO_2 film (adsorbed at 100 K) was prepared. In this and subsequent figures, curve-fitting was done with asymmetric S 2p peaks, taking into consideration the experimental resolution.

to the Redhead method,[32,33] is ~ 0.35 eV/molecule (~ 8 kcal/mol). This is in agreement with reported values for the desorption energy of multilayer SO_2 from other substrates (8 kcal/mol).[31]

Figure 2 shows a series of S 2p XPS spectra for different doses of SO_2 on polycrystalline UO_2 at 100 K. Each spectrum corresponds to a freshly prepared SO_2 film adsorbed at 100 K. The photoemission S 2p core-level spectra show peaks centered at ~ 167.8 eV. To obtain information about the chemical state of sulfur, the indicated curve fittings are done using previously published binding energy values for the different SO_x species adsorbed on several other metal oxide surfaces. Reported binding energy values for the $2p_{3/2}$ peak of SO_2, SO_3, and SO_4 (chemisorbed on metal oxides) vary from 163.0 to 165.6 eV, from 166.3 to 167.0 eV, and from 167.5 to 168.7 eV, respectively.[18,19,21,22,34] For physisorbed SO_2, S $2p_{3/2}$ values between 167.6 and 169.4 eV are reported.[21,22,35] Since the

Adsorption and Reaction of SO_2 with a UO_2 Film

J. Phys. Chem. B, Vol. 109, No. 44, 2005 **20897**

TABLE 1: Binding Energy Values for the Sulfur Components Found in the Present Experiments

SO_2 deposition onto	S 2p binding energy values (eV)						
	physisorbed SO_2	SO_4	SO_3	SO_2	S1	S2	S3
stoichiometric UO_2	168.3	168.3	167.0				
O-deficient UO_2 (adsorption at 100 K)	168.2	168.4	166.4	165.5	160.1	161.1	162.8
O-deficient UO_2 (adsorption at 300 K)			166.3		160.0	161.0	162.6
0.3 ML Ca/UO_2	168.4		167.0	165.5			
4 ML Ca/UO_2	168.4		166.6	165.5	159.7	161.0	163.2
0.4 ML Na/UO_2			166.9	165.5			
5 ML Na/UO_2			167.0	165.1	159.7	160.9	

binding energy ranges for chemisorbed SO_4 and physisorbed SO_2 overlap, the assignment of these SO_x species has to be done carefully. To consider the asymmetry of the S 2p peak (associated with the unresolved 2p spin−orbit splitting), each fitted peak shown in the following is the sum of the two peaks S $2p_{1/2}$ and S $2p_{3/2}$ separated by 1.19 eV with an intensity ratio of 1:2 (S $2p_{1/2}$:S $2p_{3/2}$) in accordance with theory. The line shape is a mixed Gaussian/Lorentzian function with a Lorentzian contribution of 30%. The S $2p_{1/2}$ and S $2p_{3/2}$ peaks have the same full width half-maximum (fwhm) of ∼2 eV.

Figure 2, curve a, shows a background spectrum for a clean uranium dioxide surface. Spectrum b was recorded after adsorption of ∼0.5 ML of SO_2 at 100 K. It consists of a single peak, whereas for higher exposures in spectra c and d a second peak on the higher binding energy side emerges. On the basis of its binding energy, the peak in spectrum b is assigned to SO_3. The additional peak in spectra c and d grows in intensity with increasing coverages, while the peak associated with SO_3 remains almost constant. Because of its higher binding energy and the fact that its intensity grows with higher coverages, the second peak is assigned to physisorbed SO_2. The S 2p binding energy values for the sulfur components of all experiments reported herein are summarized in Table 1.

Figure 3 shows a sequence of grazing angle S 2p spectra for ∼1.8 ML of SO_2 adsorbed at 100 K on polycrystalline UO_2 followed by annealing to several temperatures. During data accumulation these temperatures are kept constant. At 100 K, the photoemission S 2p core-level spectrum shows a broad peak centered at ∼168 eV. As in Figure 2, this peak consists mainly of physisorbed SO_2 and chemisorbed SO_3, as shown by the indicated curve fitting. Heating to 175 K causes a rapid decrease in the intensity of the S 2p peak; a small shift of the spectrum centroid to ∼167.5 eV is observed. This is explained by desorption of the physisorbed SO_2 molecules at ∼133 K. However at 175 K, a small peak on the higher binding energy side of the SO_3 peak persists. On the basis of its binding energy and the fact that the physisorbed layer is already desorbed (see Figure 1), this peak is assigned to chemisorbed SO_4, so that the S 2p peak at 175 K consists mainly of chemisorbed SO_3 and a small amount of SO_4.

Further heating leads to a decrease in the overall peak intensity indicating desorption of the sulfur compounds. For temperatures above 270 K the centroid of the S 2p peak shifts toward higher binding energies, which indicates that SO_4 has replaced SO_3 as the main sulfur oxide component. At 600 K, the SO_x species are desorbed and no XPS S 2p signal is found. Note also at all temperatures the absence of intensity between 161.0 and 163.5 eV, which is the typical position for atomically adsorbed sulfur.[34,36] Thus, dissociation of SO_2 does not occur on stoichiometric UO_2.

3.2. Interactions of SO_2 with Oxygen-Deficient UO_2. Since SO_2 adsorption onto stoichiometric UO_2 does not lead to the dissociation of sulfur dioxide, the creation of oxygen defects is used as a way to increase the reactivity of the polycrystalline surface. On various metal oxides the introduction of O-defects leads to the cleavage of S−O bonds on the otherwise relatively unreactive surface.[16−18,37]

Figure 4 shows U 4f XPS spectra of UO_2 after (a) Ar^+ ion sputtering, (b) deposition of SO_2 at 300 K onto the sputtered surface, (c) heating of the exposed surface to 440 K, and (d) a stoichiometric surface.

The bottom curve d taken after annealing the clean sample to 500 K for 5 min in the presence of oxygen corresponds to a film of stoichiometric UO_2. This spectrum exhibits U $4f_{5/2}$ and U $4f_{7/2}$ peaks at 390.9 and 380.1 eV, respectively; the two features located ∼6.8 eV higher in binding energies are characteristic shake-up satellites, associated with the excitation from the O 2p−U bonding band to uranium 5f states.[38,39] The positions of the U $4f_{5/2}$ and U $4f_{7/2}$ peaks as well as the positions of the shake-up satellites are in good agreement with reported values for stoichiometric UO_2.[38] The top spectrum (Figure 4a), taken after 20 min of Ar^+ ion sputtering, exhibits two new features, each located on the lower binding energy side of the U 4f peaks, and a ∼1 eV shift of the spectrum to higher binding energies (U $4f_{7/2}$ component at 381.1 eV). The feature accompanying the U $4f_{7/2}$ peak leads to a distinct shoulder, whereas the one near the U $4f_{5/2}$ peak overlaps with the shake-up satellite at this position. In accordance with reported values for the
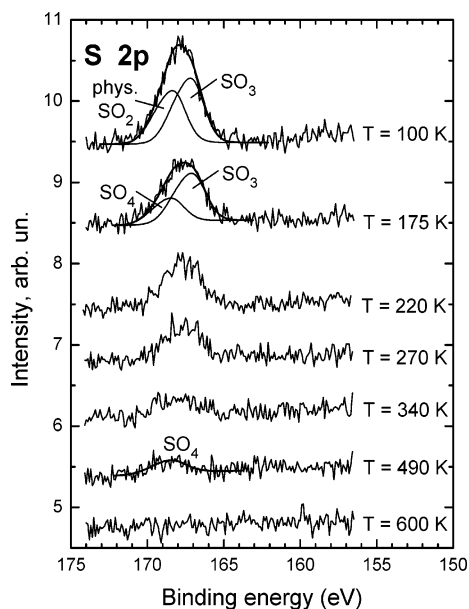

Figure 3. S 2p grazing angle XPS spectra for ∼1.8 ML of SO_2 adsorbed at 100 K on polycrystalline UO_2 followed by annealing to several temperatures. These temperatures were kept constant during data accumulation. Curve-fitting with asymmetric S 2p peaks is indicated for certain temperatures.
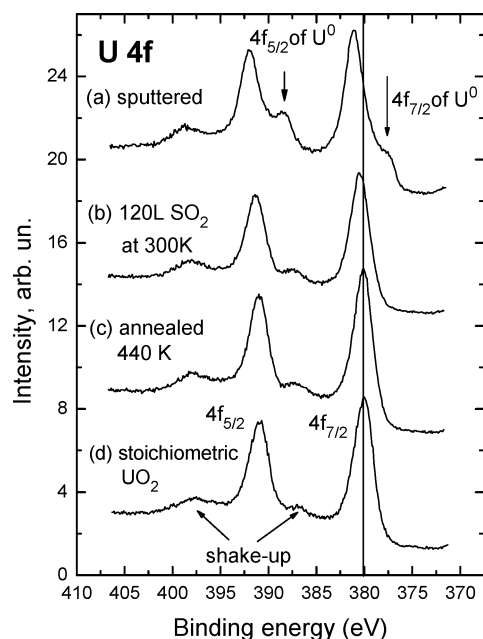
Figure 4. U 4f grazing angle XPS spectra of UO_2 after (a) Ar^+ ion sputtering, (b) deposition of SO_2 at 300 K onto the sputtered surface, (c) heating of the exposed surface to 440 K, and (d) a stoichiometric surface.

binding energies of U^0, both features are assigned to the presence of U^0 or uranium with an oxidation state close to zero.[38,40] The appearance of additional features and the peak shift after sputtering have previously been reported by Senanayake and Idriss[9] and also attributed to U^0.

The sputter-induced shift in the U 4f spectrum arises from the different electronic properties of UO_2 and UO_{2-x}. Uranium dioxide is a Mott–Hubbard insulator and, thus, theoretically, is not conducting.[41,42] However, slight deviations from stoichiometry have been shown to create positive charge carriers in the case of excess oxygen and negative charge carriers in the case of depleted oxygen.[42] Thus, hyperstoichiometric uranium dioxide is a p-type semiconductor and hypostoichiometric uranium dioxide is an n-type semiconductor; the Fermi level shifts as a result of the transition from UO_{2+x} to UO_{2-x}.[42–44] This displacement of the Fermi level from the top of the valence band to the bottom of the conduction band leads to a shift in the XPS spectra, since the Fermi level of the sample is aligned with that of the spectrometer. A similar binding energy shift of ∼1.4 eV in the O 1s spectrum (∼0.4 eV higher than that of the U 4f spectrum) is also caused by sputtering (not shown here). This can be explained by the different electronic environment of the remaining oxygen after sputtering, which leads to an additional shift. The resulting shift is the sum of the shift due to the p–n transition and the true chemical shift due to oxygen deficiency.

A shift of 1 eV between the U 4f spectra of stoichiometric and oxygen-deficient UO_2 was also seen by Van den Berghe et al.[43] and Miserque et al.[44] Winer et al.[40] and Senanayake and Idriss[9] report a shift of ∼0.8 eV in the U 4f spectrum for the transition from UO_2 to UO_{2-x}. In addition, Winer et al. also report that the O 1s shift for UO_{2-x} is ∼0.2 eV higher than that of the U 4f.

During 20 min Ar^+ ion sputtering the XPS peak area ratio O 1s/U 4f gradually decreases by ∼22%; the averaged surface stoichiometry of the sputtered surface is estimated to be UO_{2-x} with $x \sim 0.44$ (sensitivity factors and spin–orbit splitting are considered in estimating x).

After an exposure of 120 L of SO_2 onto the sputtered surface at 300 K (spectrum b in Figure 4), the U^0 features on the higher binding energy sides of the U 4f peaks are greatly attenuated and the shift in the spectrum is reduced to ∼0.4 eV (U $4f_{7/2}$ component at 380.5 eV). This indicates the filling of oxygen vacancies by incorporation of oxygen from SO_2. However the remaining core level shift and small persistent U^0 features show that even a large exposure (120 L), exceeding the monolayer saturation dose, cannot heal all the oxygen-deficient sites. This suggests that not only surface defects but also subsurface defects have been created by sputtering. After annealing the sample to 440 K (curve c) the spectrum shifts back to the position for stoichiometric UO_2 (U $4f_{7/2}$ component at 380.1 eV) and no significant difference with the spectrum for the oxygen annealed sample (stoichiometric UO_2 in Figure 4d) is seen. At this temperature the subsurface defects are believed to be healed mainly by oxygen diffusion from the bulk of the sample. Healing of O-defects in UO_2 by diffusion of oxygen during annealing was previously reported by Stultz et al.[8]

Figure 5a displays the XPS S 2p spectra for 4 ML of SO_2 dosed at 100 K onto an oxygen-deficient (Ar^+ sputtered) UO_2 sample, followed by annealing of the sample to different temperatures up to 635 K. The spectrum at 100 K exhibits a broad asymmetrical feature with a maximum at ∼168 eV. The breadth and the shape of the feature indicate that multiple states of sulfur oxides (SO_x) are present. The spectrum can be curve-fitted with three asymmetrical S 2p peaks. The fact that the signal is strongly attenuated after heating to 265 K leads to the conclusion that the main contribution to the 100 K peak is from physisorbed SO_2. This is supported by the indicated curve fitting with a large peak at binding energies characteristic for physisorbed SO_2 and two smaller peaks at lower binding energies (binding energies are given in Table 1). These two peaks are associated with chemisorbed SO_3 and SO_2 and are attenuated by ∼30% due to the considerably thick layer of physisorbed SO_2. Because the binding energy of physisorbed SO_2 overlaps with that for chemisorbed SO_4, we cannot exclude the possibility that a small fraction of SO_4 also contributes to the broad signal at 100 K. Upon heating of the sample to 265 K, the SO_x feature attenuates and its center shifts to lower binding energies exhibiting a maximum at ∼166.5 eV. Annealing to 265 K also leads to a new feature between ∼159 and ∼164.5 eV corresponding to multiple binding states of sulfur. At 300 K SO_3 is the dominant species, but also a small contribution of SO_4 exists on the oxygen-deficient surface. Further annealing over 465 K results in the attenuation of SO_x and sulfide features. The shift of the center of the SO_x peak to higher binding energies indicates that SO_4 is a persistent species, as confirmed by curve-fitting; the formation of a feature centered at ∼161.2 eV is in good agreement with reported binding energy values for atomic sulfur.[34,37] Upon further heating to 635 K both signals greatly attenuate and almost reach the background level.

The structure of the sulfur peak at lower binding energies and its behavior between 300 and 465 K is rather complex. Curve-fitting reveals two S 2p peaks (S2 (161.1 eV) and S3 (162.8 eV)) at 300 K. Upon heating of the sample to 465 K, S3 vanishes, S2 grows, and the new peak S1 (160.1 eV) emerges. The multiple S peaks may be related to different adsorption sites, as discussed in section 4.2.

Figure 5b shows the S 2p XPS spectra for sputtered UO_2 exposed to a saturation dose of SO_2 (120 L) at 300 K followed by annealing to different temperatures up to 540 K. After deposition two peaks are observed in the spectrum: one at ∼166.7 eV corresponding to adsorbed SO_3 as the dominant SO_x

Adsorption and Reaction of SO₂ with a UO₂ Film

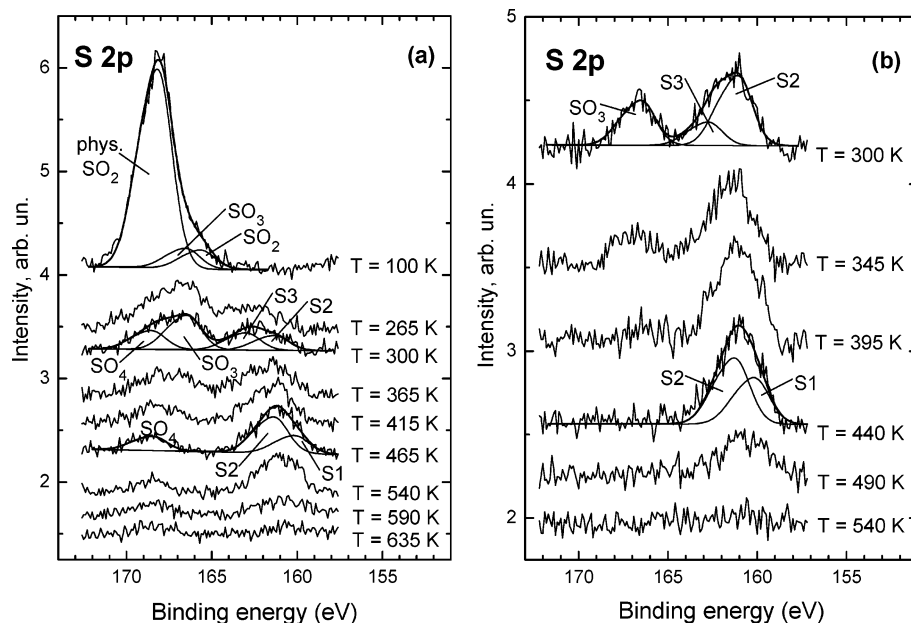*J. Phys. Chem. B, Vol. 109, No. 44, 2005* **20899**

Figure 5. S 2p grazing angle XPS spectra for (a) 4 ML of SO₂ dosed at 100 K and (b) a saturation dose of SO₂ (120 L) dosed at 300 K onto an oxygen-deficient (Ar⁺ sputtered) UO₂ sample followed by annealing of the sample at different temperatures. These temperatures were kept constant during data accumulation.
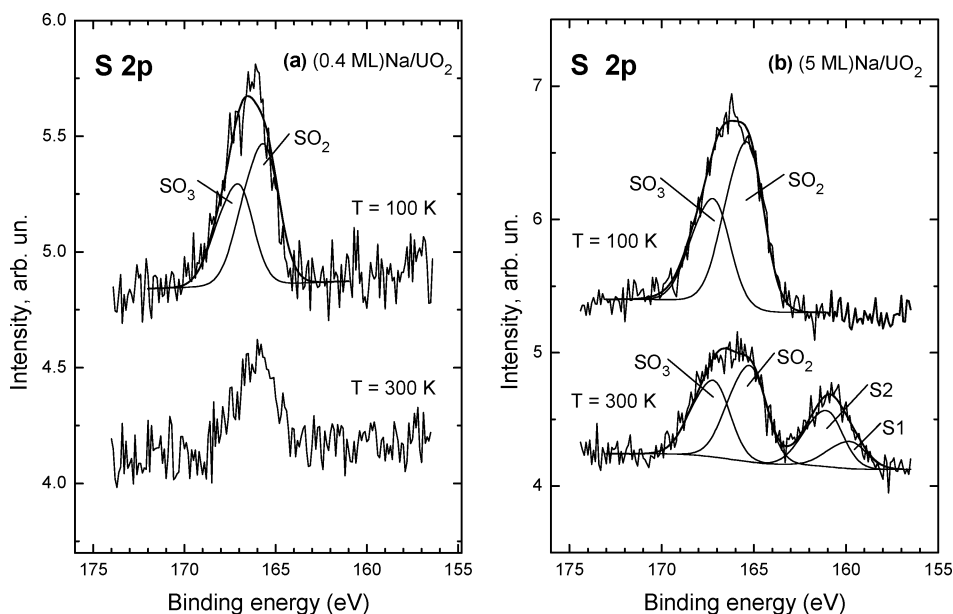

Figure 6. S 2p grazing angle XPS spectra for ~1 ML of SO₂ adsorbed at 100 K onto a UO₂ surface, which was precovered with (a) ~0.4 ML and (b) ~5 ML of sodium, followed by annealing to 300 K..

species and the other at ~161.5 eV corresponding to atomic sulfur. Upon heating, the SO_x peak decreases rapidly whereas the sulfur peak grows slightly in intensity. At a temperature of 440 K no sulfur oxide compounds are measurable and only atomic sulfur remains on the surface (at ~161 eV). Further annealing leads to desorption of sulfur, and at 540 K, no sulfur peak is observed. Similar to the spectra for deposition at 100 K, the low binding energy feature consists at 300 K of two peaks S2 (161.0 eV) and S3 (162.6 eV), and upon annealing of the sample to 440 K, S3 vanishes and a new peak S1 (160.0 eV) appears (see section 4.2). Except for this similarity, the reactions of SO₂ dosed onto O-deficient UO₂ at 300 K (Figure 5b) are somewhat different from the reactions for dosing at 100 K (Figure 5a). A large sulfur peak is observed immediately after dosing, and the SO_x species decompose completely upon heating

into oxygen (which is incorporated into the defective sites) and atomic sulfur.

3.3. Adsorption of SO₂ onto Sodium Precovered UO₂. Many studies have shown that the coadsorption of alkalis can promote the dissociation of SO₂.[16,19,21,34] This motivated us to deposit sodium onto the UO₂ surface before SO₂ adsorption, in an attempt to enhance the reactivity of uranium dioxide toward SO₂. Figure 6 shows S 2p photoemission spectra for ~1 ML of SO₂ adsorbed at 100 K onto a UO₂ surface, precovered with (a) ~0.4 ML and (b) ~5 ML of sodium, followed by annealing to 300 K. For a sodium coverage of ~0.4 ML the photoemission S 2p core-level spectrum shows after deposition at 100 K a feature that can be curve-fitted by two peaks. On the basis of the binding energy values, these two peaks are assigned to chemisorbed SO₂ and SO₃, with SO₂ as the main SO_x compo-
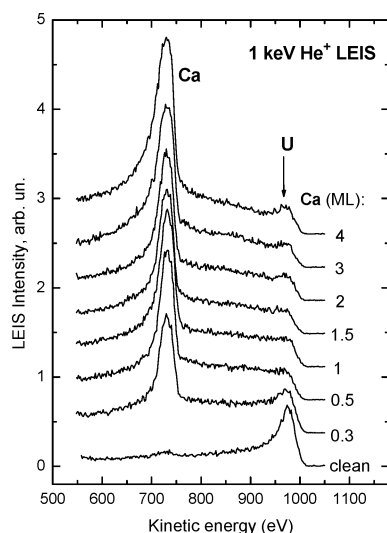
Figure 7. He^{+} LEIS spectra ($I = \sim 1$ μA) for clean UO$_2$ and different coverages of calcium on UO$_2$ (0.3−4 ML, from bottom to top). The coverages were estimated by evaluation of LEIS intensities as a function of deposition time and the attenuation of the XPS O 1s and U 4f spectra.

Figure 8. Ca 2p grazing angle XPS spectra for different amounts of calcium deposited onto UO$_2$.

nent. Upon heating of the sample to 300 K, the SO$_x$ signal intensity attenuates but still consists of a mixture of chemisorbed SO$_2$ and SO$_3$. No dissociation of SO$_2$ into sulfur and oxygen is observed on 0.4 ML Na/UO$_2$.

For a 5 ML coverage of sodium on UO$_2$ (Figure 6b), a broad peak centered at $\sim$166 eV is observed after deposition of $\sim$1 ML of SO$_2$ at 100 K. Curve-fitting reveals two asymmetrical peaks that are associated with chemisorbed SO$_2$ and SO$_3$. At 100 K chemisorbed SO$_2$ is the major SO$_x$ species on the sodium-precovered UO$_2$ surface, but a smaller amount of SO$_3$ is also present.

After heating of the sample to 300 K, the SO$_x$ peak is attenuated and a new peak at $\sim$161 eV emerges; this new peak is assigned to the presence of atomic sulfur produced by the dissociation of SO$_2$ and SO$_3$. At 300 K, chemisorbed SO$_2$, SO$_3$, and atomic sulfur coexist on the 5 ML Na/UO$_2$ surface. However, the atomic S peak is too broad to be explained by only one adsorption state. Curve-fitting indicates two different sulfur binding states S1 (159.7 eV) and S2 (160.9 eV). Whereas for 1 ML SO$_2$ on the 0.4 ML sodium-precovered surface 60% of the sulfur compounds desorb during annealing from 100 to 300 K, only 5% of them desorb from 1 ML SO$_2$ on 5 ML Na/UO$_2$ upon heating.

3.4. Adsorption of SO$_2$ onto Calcium-Precovered UO$_2$. To study the effect of an alkaline earth on the reactions of UO$_2$ with SO$_2$, we used a procedure similar to that for Na/UO$_2$: we prepared two different Ca/UO$_2$ surfaces, one with a coverage of $\sim$0.3 ML and the other with a coverage of $\sim$4 ML of calcium. For alkali metals such as Na and Cs it is well-known that adsorption of small amounts ($<$1 ML) of the alkalis onto many metal oxides leads to ionically bonded alkalis. Metallically and ionically bonded alkalis can be distinguished by differences in the XPS spectra of the substrate.[45,46] In the case of sodium on SiO$_2$ binding energy shifts in the XPS spectra of the adsorbate also provide information about the type of bonding.[47] However, the core-level binding energy differences between ionic and metallic alkaline earths are rather small,[48,49] making the distinction between ionic and metallic bonding more difficult.

Figure 7 displays the He^{+} LEIS spectra for clean and Ca-covered UO$_2$ over the coverage range from 0.3 to 4 ML. The coverages are estimated by evaluation of LEIS intensities as a function of deposition time and the attenuation of the XPS O
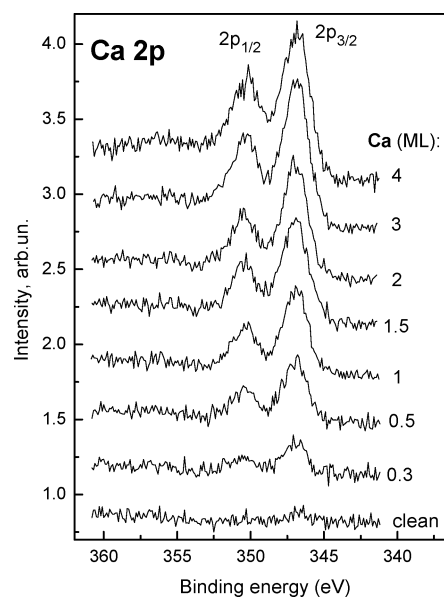
1s and U 4f peaks of the substrate. Upon deposition of 0.3 ML of calcium, the uranium peak attenuates and a new peak appears, corresponding to the scattering signal from calcium.

Further deposition of calcium leads to a reduction of the uranium peak and to a large increase in the calcium peak. The difference in height between the uranium peak and the calcium peak results from the different scattering cross sections for calcium and uranium and is not a measure of the quantitative composition of the surface. The high background on both sides of the Ca peak is attributed to multiple scattering of He^{+} on the rough Ca-covered surface. Due to the high neutralization probability during the scattering process, multiply scattered He^{+} ions are expected to be neutralized efficiently and not contribute to the LEIS spectrum. However, calcium has been reported to largely enhance the reionization probability of He neutralized in the scattering event.[50] It is also important to note that even at high coverages of calcium (4 ML) a uranium signal persists, suggesting the growth of calcium clusters.

Figure 8 shows Ca 2p XPS spectra for different amounts of calcium deposited on UO$_2$. The Ca 2p spectra show both the 2p$_{1/2}$ peak at 350.3 eV and the 2p$_{3/2}$ peak at 346.9 eV; no significant shift for increasing calcium deposition is visible. The increased background on the higher binding energy side and the broadening of the spectra for Ca coverages $>$1 ML is a result of the plasmon excitations, which are typical for metals.[51] The deposition of Ca coverages larger than 1 ML leads to metallic calcium whereas the deposition of 0.3 ML leads to ionically bonded Ca; the evidence for ionic bonding is not obvious from the XPS spectra, but theoretical analysis leads to the conclusion that despite the small shift in binding energies, the bonding of calcium with oxygen atoms, which are believed to be the preferential adsorption sites, must be regarded as highly ionic.[48]

Figure 9 shows the S 2p XPS spectra for SO$_2$ adsorption ($\sim$1.3 ML) at 100 K onto a UO$_2$ surface that was precovered (at 300 K) with (a) $\sim$0.3 ML and (b) $\sim$4 ML of calcium. After adsorption of SO$_2$, the Ca/UO$_2$ surfaces were annealed to the various temperatures indicated and the corresponding spectra were recorded at these temperatures. The top spectrum in Figure 9a exhibits a broad feature centered at $\sim$167.3 eV corresponding to multiple SO$_x$ species. This peak can be curve-fitted by three
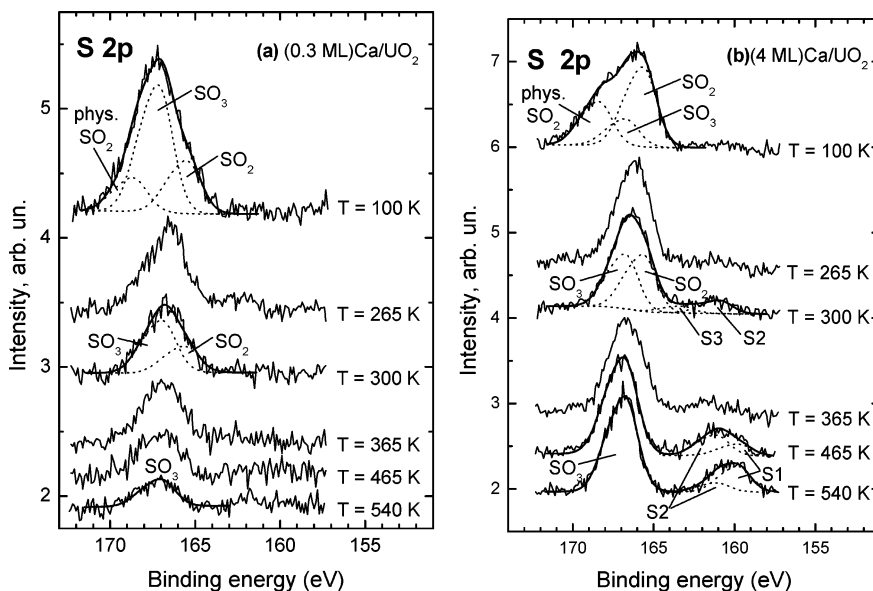
Adsorption and Reaction of SO$_2$ with a UO$_2$ Film

J. Phys. Chem. B, Vol. 109, No. 44, 2005 **20901**

Figure 9. S 2p grazing angle XPS spectra for SO$_2$ deposition (~1.3 ML) at 100 K onto a UO$_2$ surface, which was precovered (at 300 K) with (a) ~0.3 ML and (b) ~4 ML of calcium, followed by annealing to various temperatures. The spectra were recorded at constant temperature.

asymmetrical S 2p peaks of which the two that are lower in binding energy are assigned to chemisorbed SO$_2$ and SO$_3$.

The attenuation of the SO$_x$ feature and the vanishing of the third peak upon heating to 265 and 300 K suggest that this third peak corresponds to physisorbed SO$_2$. After annealing of the sample to 300 K the still broad, attenuated peak is centered at ~166.5 eV and consists of chemisorbed SO$_2$ and SO$_3$. Upon further annealing the SO$_x$ peak shifts slightly to higher binding energies, and at 540 K it is centered at ~167.0 eV. Curve-fitting indicates that SO$_3$ is the only sulfur oxide species on the surface. For temperatures over 365 K a very small enhancement in the background signal is seen between 159 and 163 eV, which might be associated with atomic sulfur from the dissociation of small amounts of SO$_2$ or SO$_3$ (estimated coverage of atomic sulfur < 0.05 ML).

The spectrum for SO$_2$ adsorption at 100 K onto 4 ML of calcium on UO$_2$ (Figure 9b) shows a broadened peak between 163.5 and 171.0 eV, which can be curve-fitted by three S 2p peaks. Upon heating of the sample to 265 and 300 K, physisorbed SO$_2$ disappears whereas chemisorbed SO$_2$ and SO$_3$ remain. Already at 265 K, a small bump between 159 and 163 eV corresponding to atomic sulfur is visible; this feature grows upon further annealing. During annealing to 540 K the sulfur oxide peak narrows and shifts to higher binding energies, ~167.0 eV, the SO$_2$ peak (chemisorbed) disappears, and only SO$_3$ remains. The atomic sulfur peak grows in intensity and shifts to its final position with its center at ~160.3 eV. It is important to note that from 100 to 300 K the sum of the peak areas for the chemisorbed species remains constant within experimental uncertainty; just the SO$_3$/SO$_2$ area ratio changes from ~0.35 to ~0.95. Upon heating of samples to temperatures higher than 300 K, the area of the SO$_x$ peak drops only slightly (by the same amount the sulfide peak is growing) and reaches at 540 K ~90% of its original value (at 265 K) with SO$_3$ as the only sulfur oxide species. The total fraction of desorbed sulfur compounds after heating to 540 K is less than 5%. The low binding energy feature shows behavior similar to that for SO$_2$ deposition onto O-deficient UO$_2$. It consists of the two peaks S2 (161.0 eV) and S3 (163.2 eV) at 300 K, and during heating to 540 K, S3 disappears whereas the new peak S1 (159.7 eV) emerges.

4. Discussion

4.1. Adsorption and Desorption of SO$_2$ on Stoichiometric UO$_2$. Sulfur dioxide (adsorbed at 100 K) is found to desorb molecularly from UO$_2$ upon heating, with the peak temperature for desorption of the physisorbed multilayer at ~133 K (Figure 1). The interpretation of the peaks at higher temperatures is not straightforward, since, after the desorption of physisorbed SO$_2$, only SO$_3$ and SO$_4$ species are present on the surface (see discussion of XPS results below). Thus, the SO$_2$ desorption rate at higher temperatures is limited by the decomposition of SO$_3$ and SO$_4$ into SO$_2$. XPS results (see below) indicate that, between 175 and 270 K, SO$_3$ and SO$_4$ decrease simultaneously and a transformation from SO$_3$ into SO$_4$ occurs for temperatures higher than 270 K. Therefore, for $T > 340$ K, mainly SO$_4$ is left on the surface, which decomposes and desorbs as SO$_2$ upon heating. Because of the complex chemistry that contributes to the shape of the high-temperature desorption peaks, a simple Redhead treatment[32,33] for determining the desorption energy is not possible. Since the majority species is SO$_4$ for $T > 340$ K, the desorption peaks with leading edge at temperatures higher than 340 K (these are the spectra in Figure 1 for coverages between 0.01 and 0.05 ML) can be assigned to the decomposition of chemisorbed SO$_4$ into SO$_2$ followed by desorption of SO$_2$. The features between multilayer desorption and 340 K belong to a mixture of SO$_3$ and SO$_4$ decomposition as a result of the complex interaction of these chemisorbed SO$_x$ species with UO$_2$ during heating.

The XPS spectra in Figure 2 show that SO$_2$ adsorbs onto UO$_2$ at 100 K as an SO$_3$ complex, which is accompanied by physisorbed SO$_2$ at higher coverages; there is no evidence for chemisorbed SO$_2$ (peak expected between 163.0 and 165.6 eV). Upon heating of the samples to 175 K, physisorbed SO$_2$ desorbs and at higher temperatures chemisorbed SO$_4$ appears (Figure 3). Although the main feature itself attenuates, the peak area ratio SO$_3$/SO$_4$ remains almost constant between 175 and 270 K, which indicates that SO$_3$ and SO$_4$ decompose and uniformly desorb in this temperature range. For temperatures over 270 K, the peak position suggests SO$_4$ to be the major SO$_x$ species on the UO$_2$ surface. At a temperature of 600 K all SO$_x$ species are desorbed, in agreement with the TPD measurements. No dissociation of sulfur dioxide into sulfur and oxygen is seen at

any temperature. Thus, the formation of SO_3 at 100 K and of SO_4 at higher temperatures may be due to the interaction of SO_2 with the oxygen centers of the UO_2 surface via the reaction:[19,21]

$$SO_{2,gas} + nO_{surf} \rightarrow SO_{2+n,ads} \quad n = 1, 2$$
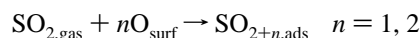
Since no chemisorption of SO_2 is seen, we conclude that the corresponding interaction of SO_2 with the metal sites[21,22,52] is weaker than the interaction with the oxygen sites of the surface, which are the adsorption sites associated with the formation of SO_3 and SO_4 species.[16,22] The presence of steps and lattice defects in the polycrystalline UO_2 sample enhance the formation of SO_3 and SO_4-like species by increasing the number of low-coordinated oxygen atoms. The presence of SO_4 as the major sulfur oxide species for $T > 270$ K can be explained by preferential desorption of SO_3 at higher temperatures or temperature-dependent transformation of SO_3 into SO_4 via reaction of SO_3 with surface oxygen atoms. This transformation can be induced by the increased accessibility of low-coordinated oxygen atoms due to enhanced mobility of the chemisorbed compound or lattice deformations at elevated temperatures.[22]

Our results are similar to reported reactions of SO_2 with several other metal oxides. For MgO(100),[22,34] there is also no evidence for chemisorption of SO_2 at low temperature; instead, SO_3 is the main sulfur oxide species reported for this surface. For $TiO_2(100)$[37] and $TiO_2(110)$[52] a thermally activated two-step reaction with SO_3 as intermediate product is reported, followed by the transformation into SO_4 as the stable end product. For adsorption at higher temperatures, SO_4 is also seen on ZnO,[19] CeO_2,[18] and α-Fe_2O_3[53] as the principal stable SO_x compound.

4.2. Basic Principles for the Cleavage of S−O Bonds and Interactions of SO_2 with Oxygen-Deficient UO_2. The dissociation of adsorbed SO_2 occurs via weakening of the S−O bonds by charge transfer from the substrate to the antibonding LUMO of SO_2. Such a charge transfer is difficult on oxide substrates due to the low electron density on the metal cations. However, it is possible to enable a metal oxide to cleave S−O bonds by creation of occupied metal states above the valence band of the oxide by creating oxygen vacancies, coadsorbing alkali metals, or doping with a transition metal.[16] In Figure 10 energy level diagrams for the bands of stoichiometric UO_2 and the molecular orbitals (MO) of SO_2 are shown.

In addition, Figure 10 shows the atomic orbital (AO) levels of U^0, Na, Ca and Ca^+, and the tops of the conduction bands of metallic U, Na, and Ca. The highest occupied atomic orbital levels of U^0, Na, and Ca as well as the tops of the conduction bands of metallic U, Na, and Ca are closer to the LUMO of SO_2 than the top of the $U 5f^2$ band of UO_2, whereas the highest occupied levels of ionically bonded Na and Ca are below the top of the highest occupied UO_2 band. It is important to note that the atomic orbital levels of adsorbed atoms are broadened due to substrate−adsorbate level-mixing. As a result of image charge effects, they are shifted closer to the Fermi level than the ones shown in Figure 10, which are the AO levels for the free atoms.[57] Furthermore the atomic levels due to charge transfer to the substrate are not completely filled. However, this donation of charge into substrate levels can also provide occupied states above the valence band of UO_2. Therefore, the presence of neutral Na or Ca atoms or metallic Na or Ca can promote charge transfer into the LUMO of SO_2 and lead to the dissociation of SO_2; ionic Na or Ca is not able to facilitate dissociation. The description of the changes in the electronic properties of the UO_2 surface induced by Ar^+ ion sputtering in terms of an energy level diagram is more complex. Since
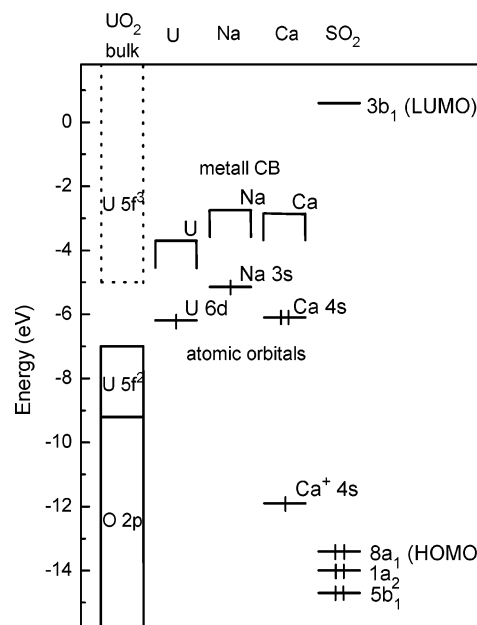
Figure 10. Energy level diagram showing UO_2 bands,[44,54] molecular orbital levels of SO_2,[19] atomic orbital levels of U^0, Na, Ca, and Ca^+,[55,56] and the top of the conduction bands of metallic U, Na, and Ca. The energy values are referenced to the vacuum level. The energy ranges of the UO_2 bands have been calculated from data referenced to the Fermi level.[44,54] Because the work function of UO_2 is not known exactly, the UO_2 bands plotted should be viewed as an approximation. The empty and occupied states of stoichiometric UO_2 are indicated by dotted lines and solid lines, respectively.

sputtering of UO_2 can lead to isolated defects but also to small clusters of metallic uranium, the highest occupied level lies between the two limiting cases of atomic U^0 and metallic uranium. This position is closer to the LUMO than the $U 5f^2$ band of UO_2, so that the creation of reduced uranium enhances the ability of UO_2 to dissociate SO_2. In the experiments discussed in this section, oxygen defects were created before SO_2 adsorption.

The changes in the U 4f XPS spectra caused by Ar^+ ion sputtering (Figure 4a) have been discussed in section 3.2 and are known to be related to the surface stoichiometry. Even after exposure to high doses of oxygen-containing molecules (120 L of SO_2), the U 4f XPS spectrum (Figure 4b) still shows features for reduced UO_2; this observation is interpreted as follows. Sulfur dioxide can heal only the outermost surface layer by dissociation into sulfur and oxygen. Thus, subsurface defects created during Ar^+ ion sputtering are responsible for the persistence of reduced UO_2 features after SO_2 adsorption. The creation of subsurface defects is possible due to preferential sputtering of oxygen, as observed on many metal oxides. Preferential sputtering is in general more pronounced for oxides containing more massive metals.[58] The subsurface defects can be healed by annealing to 440 K, where oxygen atoms diffuse from the bulk of the sample to the defect sites.[8]

The Ar^+ ion sputtering also has a dramatic influence on the reactivity of UO_2 toward SO_2, as shown in Figure 5. In contrast to adsorption on stoichiometric UO_2 not only SO_3 and physisorbed SO_2 but also chemisorbed SO_2 is present at 100 K (Figure 5a). This indicates that the interaction of SO_2 with the metallic centers is increased due to the lack of oxygen. An interpretation of the presence of chemisorbed SO_2 is that the formation of the SO_3 complex on UO_2 may happen in two steps similar to the mechanism proposed for MgO,[22] where first a bonding between SO_2 and the metal centers is established (inducing a weakening of the metal−oxygen bond in the

Adsorption and Reaction of SO₂ with a UO₂ Film

J. Phys. Chem. B, Vol. 109, No. 44, 2005 **20903**

substrate), followed by SO_2 bonding to the oxygen sites of the oxide. The reduced concentration of oxygen in the substrate may cause the reaction to stop at low temperatures in the first step, resulting in chemisorbed SO_2. The physisorbed SO_2 desorbs upon heating, followed by desorption of the chemisorbed SO_2 below 300 K. A distinct sulfur signal appearing at 265 K indicates that a fraction of the SO_2 dissociates completely on O-deficient UO_2. The disappearance of the chemisorbed SO_2 peak results not only from desorption but also from dissociation. Unlike stoichiometric UO_2, the formation of chemisorbed SO_4 on the oxygen-deficient surface may not be from the reaction of SO_2 or SO_3 with substrate oxygen; rather, it may be associated with the reaction of SO_2 and SO_3 with oxygen atoms produced by SO_2 dissociation. Between 300 and 465 K the amount of atomic sulfur increases whereas the amount of SO_x species decreases; a decrease in the SO_3/SO_4 peak area ratio is also observed in this temperature range. This indicates that, in addition to the simple desorption, two types of reactions may occur: (a) the direct dissociation of SO_3 and (at higher temperatures) SO_4 into sulfur and oxygen; (b) the transformation of SO_3 into SO_4 caused in part by the reaction of SO_3 with oxygen atoms from completely dissociated SO_x. The end products for adsorption on the reduced surface are thermally more stable than those for adsorption on stoichiometric UO_2.

For deposition at 300 K, displayed in Figure 5b, atomic sulfur and SO_3 coexist on the oxide surface immediately after dosing. At 440 K the SO_x species are entirely dissociated and only atomic sulfur is left on the oxide surface. Upon heating of the sample to 540 K the accumulated sulfur desorbs completely. The large intensity at the position for atomic sulfur and the fact that heating produces no SO_4 signal indicates that the chemistry for SO_2 adsorption at 300 K onto hypostoichiometric UO_2 is different from that at 100 K. For SO_2 deposition at 100 K on O-deficient UO_2, followed by heating, two different reactions are believed to occur, namely the dissociation of SO_2 and the formation of SO_4 via the reaction of SO_2 and SO_3 with oxygen atoms from dissociated SO_2. In contrast, for deposition at 300 K on O-deficient UO_2 followed by heating, the dissociation of SO_2 is the preferred reaction. For deposition at 300 K no physisorbed SO_2 layer accumulates; only a small amount of SO_x is chemisorbed on the surface, and the system has enough thermal energy to dissociate SO_2 readily during the adsorption process, whereas for adsorption at 100 K SO_2 is mainly physisorbed. The smaller SO_x concentration and in particular the absence of the large physisorbed SO_2 layer might be the reasons for suppression of SO_4 formation after SO_2 deposition at 300 K. Thus, only the dissociation reaction occurs; SO_2 dissociates directly upon adsorption until all reactive centers are occupied with sulfur or oxygen. Upon heating, oxygen diffuses into the reduced subsurface region and thus produces new active sites for the dissociation of chemisorbed SO_3.

Because of its breadth, the interpretation of the atomic sulfur peak (Figure 5) is not straightforward. During annealing a trend to lower binding energies is observed. One interpretation for the peaks S1, S2, and S3 is that they correspond to different adsorption sites and geometries. The polycrystalline UO_2 sample exhibits numerous defects that can provide different adsorption sites. Since no XPS data for SO is available, we cannot exclude the possibility that the peak with the highest binding energy (S3) may be related to sulfur coordinated to only one oxygen atom. Another possible interpretation is the presence of polyatomic sulfur molecules (S_n) as reported for adsorption of sulfur onto different metal surfaces.[59,60] In these cases evidence for the presence of S_2, S_4, and S_8 is seen.

Sputtering of UO_2 leads to uranium in a low oxidation state (U^0). The metal cations in a reduced oxidation state can provide occupied electronic states above the valence band of the metal oxide[16,61] (see Figure 10) that are needed for the interaction with the LUMO of SO_2. After both experiments (deposition at 100 K and at 300 K) the surface stoichiometry is restored, as confirmed by XPS measurements. The healing of O-defects occurs in two steps: (1) incorporation of oxygen atoms from dissociated SO_x at temperatures lower than 440 K; (2) diffusion of oxygen atoms from the bulk of the sample to the defective sites during annealing to temperatures higher than 440 K. This is supported by the fact that for temperatures higher than 465 K no further dissociation but only desorption of sulfur components is observed.

The creation of oxygen defects has also been used successfully to enhance the reactivity of several other metal oxides toward SO_2. On MgO the existence of surface and subsurface oxygen vacancies was seen to be important for S−O bond cleavage.[16] Also on CeO_2,[18] NiO(100),[17] and TiO_2(100),[34] dissociation of SO_2 was seen only after the introduction of oxygen defects.

4.3. Adsorption of SO₂ onto Sodium-Precovered UO₂. Coadsorption of sodium with SO_2 was used in an attempt to increase the ability of stoichiometric UO_2 to dissociate SO_2. We prepared two Na/UO_2 surfaces, one with a sodium coverage of 0.4 ML and the other with a sodium coverage of 5 ML. Complete dissociation of SO_2 is only seen for a coverage of 5 ML of sodium on UO_2.

Almost invariably, evidence for SK (Stranski−Krastanov) or layer growth is seen for alkali adsorption on metal oxides.[45] Sodium adsorbs in ionic form for small coverages on many metal oxides and metallic sodium forms with increasing coverage.[45,47] Thus, for a coverage of 0.4 ML, sodium is expected to form ionic bonds with the UO_2 substrate. A coverage of 5 ML of sodium produces metallic sodium. The XPS results for adsorption of SO_2 onto Na/UO_2 at 100 K (Figure 6) show a mixture of SO_2 and SO_3 for both sodium coverages (0.4 and 5 ML). However, the ratio SO_2/SO_3 is higher (by about 15%) in the case of 5 ML sodium coverage. Upon heating of the sample to 300 K, about 60% of the sulfur species on 0.4 ML Na/UO_2 desorb, whereas on 5 ML Na/UO_2, 95% of the sulfur species remain on the substrate in form of SO_2, SO_3, and atomic sulfur (from complete dissociation). The absence of the SO_4 peak and the appearance of chemisorbed SO_2, even at a low coverage of sodium (0.4 ML), suggest that Na preferentially bonds to oxygen and thus blocks the O sites for interaction with SO_2, which leads to a decrease in SO_3 and SO_4 production and to the formation of chemisorbed SO_2 (as discussed above for oxygen-deficient UO_2). Oxygen as the preferred adsorption site for sodium was also reported for TiO_2(110)[62] and MgO.[63] For the 0.4 ML Na/UO_2 system, the appearance of SO_3 can be explained by reaction of SO_2 with oxygen atoms of UO_2 (similar to stoichiometric UO_2). For a coverage of 5 ML of sodium, however, the surface is covered completely with sodium, and no interactions with surface oxygen should be possible. Thus, the presence of SO_3 must be explained by another mechanism that provides the needed oxygen. The amount of SO_3 observed is too big to be caused by reaction of SO_2 with oxygen of the residual gas. Formation of SO_3 without sufficient oxygen concentration was also observed for SO_2 deposition onto the metals Zn[64] and Sn[65] and explained by the proposed disproportionation reaction:

$$2SO_{2,ads} \rightarrow SO_{gas} + SO_{3,ads}$$

It is, however, important to note that so far no reports confirming the SO gas evolution upon SO_2 deposition on these metals are available. The disproportionation reaction may also be the dominating pathway for the formation of SO_3 on the 5 ML Na/UO_2 surface. The minor change in sulfur compound coverage after heating to 300 K indicates the enhanced ability of the surface to bind SO_x and sulfur species; during heating, SO_x decomposes into oxygen and sulfur almost without desorption of sulfur components. The low desorption during heating of the 5 ML Na/UO_2 surface can be explained by increased adsorption energy due to the smaller energy separation between Na and SO_2 LUMO level compared to the separation between the $5f^2$ band of UO_2 and the SO_2 LUMO level (see Figure 10) and was also seen for Cs/ZnO[19] and $Na/MgO(100)$.[34] The bonding energy is roughly proportional to $1/(E_{LUMO} - E_{AS})$;[19] the smaller the separation between the LUMO level of SO_2 E_{LUMO} and the adsorption site level E_{AS}, the higher is the bonding energy. The position of the sulfide peaks S1 and S2 are similar to that observed for SO_2 on the oxygen-deficient UO_2 surface.

The ability of high coverages of alkali metals on oxides to dissociate SO_2 was seen on several other systems.[16,19,21,34] However, unlike Na/MgO,[16,34] Cs/ZnO,[19] and K or Cs/ZnO-$(000\bar{1})$-O,[21] sodium on UO_2 does not promote S–O bond cleavage for small coverages (<1 ML) of the alkali. Alkalis interact strongly with a narrow-band gap oxide substrate, which leads to a charge transfer from the alkali to the oxide and to reduction of the substrate metal cations.[45,66] Therefore, the interactions of UO_2 (band gap 2.1–2.7 eV[42,43]) with sodium are very strong and cause a charge transfer from sodium to UO_2. For small coverages of Na (<1 ML) this leads to ionic sodium[45,47,66] and thus reduces the density of occupied states (from metallic sodium) above the valence band that are necessary to enhance the interaction of the substrate with the LUMO of SO_2 (see Figure 10). On the other hand, the reduction of uranium cations due to alkali adsorption may not be strong enough to provide electronic states that can transfer charge carriers into the LUMO of SO_2, unlike what was seen for alkali deposition onto TiO_2.[45] The absence of metallic sodium and sufficiently reduced uranium at low alkali coverage therefore leads to a surface that is not able to decompose SO_2. After heating of the sample to 300 K, the sulfur species on both surfaces (0.4 ML Na/UO_2 and 5 ML Na/UO_2) may be bonded as various compounds, such as Na_xSO_y complexes, and for a sodium coverage of 5 ML also in form of sodium sulfides and oxides. The formation of these Na compounds might also explain why no transformation of SO_3 into SO_4 is observed upon heating in contrast to the experiments with stoichiometric and O-deficient UO_2 (Figures 3 and 5).

4.4. Adsorption of SO_2 onto Calcium-Precovered UO_2. We have studied the adsorption of SO_2 onto UO_2 surfaces precovered with different amounts of calcium (0.3 and 4 ML), to examine the influences of earth alkali metals on oxide reactivity. Sulfur dioxide dissociates only on the UO_2 surface precovered with a large coverage (4 ML) of calcium.

For deposition of SO_2 at 100 K onto 0.3 ML Ca/UO_2, physisorbed SO_2 as well as chemisorbed SO_2 and SO_3 are present. In contrast to the Na/UO_2 system, SO_3 is the major sulfur oxide species. Since the calcium coverage of 0.3 ML is comparable to the sodium coverage of 0.4 ML, this might indicate that oxygen sites are not as strongly blocked by calcium as by sodium. Heating leads to desorption of physisorbed SO_2 followed by chemisorbed SO_2 and SO_3. Since only SO_3 remains on the surface at 540 K, a transformation from SO_2 into SO_3

by reaction of SO_2 with oxygen atoms of the substrate oxide cannot be excluded. Sulfur dioxide deposition at 100 K onto 4 ML Ca/UO_2 leads to the same three products, but for this surface chemisorbed SO_2 represents the main SO_x compound. We conclude that at this coverage calcium greatly reduces the interactions between the oxide surface and SO_2. The small amount of SO_3 produced may result, like on the 5 ML Na/UO_2 system, mainly from the disproportionation reaction rather than from reaction of SO_2 with surface oxygen (see section 4.3). Similar to sodium, calcium on UO_2 can also increase the adsorption energy of sulfur compounds; the small amount of desorption (less than 5%) of sulfur species during heating of the 4 ML Ca/UO_2 surface is analogous to Na/UO_2 and is associated with the small energy separation between Ca (metallic) and SO_2 LUMO level, leading to a high adsorption energy. This low amount of desorption, the disappearance of chemisorbed SO_2 upon heating, and the continuous growth of the SO_3 and sulfide signals for temperatures higher than 100 K suggest the complete dissociation of SO_2 and a transformation of SO_2 into SO_3 via reaction of SO_2 with oxygen atoms from SO_2 dissociation. The transformation of SO_3 into SO_4 is suppressed by the reduced accessibility of surface oxygen and by the competing reaction of oxygen with calcium. The structure of the sulfide peak consisting of the peaks S1, S2, and S3 is similar to that observed for SO_2 on oxygen-deficient UO_2 (section 4.2). The sulfur species may form various compounds with Ca on both surfaces (0.3 ML Ca/UO_2 and 4 ML Ca/UO_2). These may include Ca_xSO_y complexes and for a calcium coverage of 4 ML also calcium sulfides and oxides.

Only large coverages of calcium lead to the cleavage of S–O bonds, supporting the conclusion that metallic states above the valence band of a metal oxide are, unlike ionic states, able to interact with the LUMO of SO_2 and weaken S–O bonds thus leading to dissociation of SO_2 (see Figure 10). Also the reduction of uranium by ionic calcium for small coverages of the earth alkali is not strong enough to provide these necessary states. Thus, a fractional monolayer of calcium is not a good promoter for the dissociation of SO_2 on UO_2.

5. Conclusion

The interactions of SO_2 with stoichiometric, oxygen-deficient, sodium-precovered and calcium-precovered UO_2 have been examined. On stoichiometric UO_2, sulfur dioxide adsorbs as SO_3 via reaction with surface oxygen. Heating leads to a transformation into SO_4, but no dissociation is observed. Argon ion sputtering of UO_2 leads to the formation of surface and subsurface oxygen defects. The surface oxygen vacancies can be healed by adsorption of SO_2. After sputtering the U 4f XPS spectra exhibit two new features corresponding to the presence of uranium with a low oxidation state and a shift in binding energies due to a p–n transition that UO_2 undergoes during sputtering. On oxygen-deficient UO_2 complete dissociation of SO_2 is observed and the reaction starts at temperatures as low as 265 K. Sulfur dioxide adsorbs onto oxygen-deficient UO_2 in the form of chemisorbed SO_2 and SO_3 at 100 K and transforms during annealing into SO_4 and atomic sulfur. At 300 K SO_2 dissociates readily during adsorption and small amounts of SO_3 are seen.

On both sodium- and calcium-precovered UO_2, sulfur dioxide adsorbs as chemisorbed SO_2 and SO_3. On the Ca/UO_2 system a transformation into SO_3 is observed upon heating. For both systems (Na/UO_2 and Ca/UO_2) dissociation of SO_2 is only seen for large coverages (≥4 ML) of the coadsorbed metal. The adsorption of large coverages of sodium or calcium also greatly enhances the adsorption energy of sulfur components.

Adsorption and Reaction of SO$_2$ with a UO$_2$ Film

J. Phys. Chem. B, Vol. 109, No. 44, 2005 **20905**

The atomic sulfur peak shows similar structure in all cases where dissociation occurs; three different binding states are observed. These could correspond to different adsorption sites on the polycrystalline sample or to sulfur molecules in different polyatomic modifications (S$_n$).

References and Notes

(1) *DOE/EIS-026*; U.S. Department of Energy; Office of Nuclear Energy, Science, and Technology: 1999.

(2) Dubrin, J. W. *UCRL-AR-124080*; Lawrence Livermore National Laboratory: Livermore, CA, 1997**;** V. 1, Rev. 2.

(3) *Depleted Uranium Hexafluoride Management Program: Depleted Uranium Hexafluoride Fact Sheet*; U.S. Department of Energy, Office of Environmental Management: Springfield, VA, 2001.

(4) Hutchings, G. J.; Heneghan, C. S.; Hudson, I. D.; Taylor, S. H. *Nature* **1996**, *384*, 341.

(5) Heneghan, C. S.; Hutchings, G. J.; O'Leary, S. R.; Taylor, S. H.; Boyd, V. J.; Hudson, I. D. *Catal. Today* **1999**, *54*, 3.

(6) Gordeeva, L. G.; Aristov, Y. I.; Moroz, E. M.; Rudina, N. A.; Zaikovskii, V. I.; Tanashev, Y. Y.; Parmon, V. N. *J. Nucl. Mater.* **1995**, *218*, 202.

(7) Hedhili, M. N.; Yakshinskiy, B. V.; Madey, T. E. *Surf. Sci.* **2000**, *445*, 512.

(8) Stultz, J.; Paffett, M. T.; Joyce, S. A. *J. Phys. Chem. B* **2004**, *108*, 2362.

(9) Senanayake, S. D.; Idriss, H. *Surf. Sci.* **2004**, *563*, 135.

(10) Chong, S. V.; Idriss, H. *Surf. Sci.* **2002**, *504*, 145.

(11) Chong, S. V.; Barteau, M. A.; Idriss, H. *Catal. Today* **2000**, *63*, 283.

(12) Wu, Q.; Yakshinskiy, B. V.; Madey, T. E. *Surf. Sci.* **2003**, *523*, 1.

(13) Wu, Q.; Yakshinskiy, B. V.; Gouder, T.; Madey, T. E. *Catal. Today* **2003**, *85*, 291.

(14) Hedhili, M. N.; Yakshinskiy, B. V.; Schlereth, T. W.; Gouder, T.; Madey, T. E. *Surf. Sci.* **2005**, *574*, 17.

(15) Stern, A. C.; Boubel, R. W.; Turner, D. B.; Fox, D. L. *Fundamentals of air pollution*, 2nd ed.; Academic Press: Orlando, FL, 1984.

(16) Rodriguez, J. A.; Jirsak, T.; Gonzalez, L.; Evans, J.; Perez, M.; Maiti, A. *J. Chem. Phys.* **2001**, *115*, 10914.

(17) Li, X.; Henrich, V. E. *Phys. Rev. B* **1993**, *48*, 23.

(18) Rodriguez, J. A.; Jirsak, T.; Freitag, A.; Hanson, J. C.; Larese, J. Z.; Chaturvedi, S. *Catal. Lett.* **1999**, *62*, 113.

(19) Rodriguez, J. A.; Jirsak, T.; Hrbek, J. *J. Phys. Chem. B* **1999**, *103*, 1966.

(20) Jirsak, T.; Rodriguez, J. A.; Hrbek, J. *Surf. Sci.* **1999**, *426*, 319.

(21) Rodriguez, J. A.; Jirsak, T.; Chaturvedi, S.; Kuhn, M. *Surf. Sci.* **1999**, *442*, 400.

(22) Rodriguez, J. A.; Jirsak, T.; Freitag, A.; Larese, J. Z.; Maiti, A. *J. Phys. Chem. B* **2000**, *104*, 7439.

(23) Triguero, L.; de Carolis, S.; Baudin, M.; Wojcik, M.; Hermansson, K.; Nygren, M. A.; Pettersson, L. G. M. *Faraday Discuss.* **1999**, *114*, 351.

(24) de Carolis, S.; Pascual, J. L.; Pettersson, L. G. M.; Baudin, M.; Wojcik, M.; Hermansson, K.; Palmqvist, A. E. C.; Muhammed, M. *J. Phys. Chem. B* **1999**, *103*, 7627.

(25) Yates, J. T., Jr. *Experimental Innovations in Surface Science*; Springer-Verlag: New York, 1998; p 644.

(26) Höfer, M.; Stolz, H.; Wassmuth, H.-W. *Surf. Sci.* **1992**, *272*, 342.

(27) Polcik, M.; Wilde, L.; Haase, J.; Brena, B.; Cocco, D.; Comelli, G.; Paolucci, G. *Phys. Rev. B* **1996**, *53*, 13720.

(28) Ahner, J.; Effendy, A.; Vajen, K.; Wassmuth, H.-W. *Vacuum* **1990**, *41*, 98.

(29) Sun, Z.-J.; Gravelle, S.; Mackay, R. S.; Zhu, X.-Y.; White, J. M. *J. Chem. Phys.* **1993**, *99*, 10021.

(30) Liu, G.; Rodriguez, J. A.; Dvorak, J.; Hrbek, J.; Jirsak, T. *Surf. Sci.* **2002**, *505*, 295.

(31) Rodriguez, J. A.; Perez, M.; Jirsak, T.; Evans, J.; Hrbek, J.; Gonzalez, L. *Chem. Phys. Lett.* **2003**, *378*, 526.

(32) de Jong, A. M.; Niemantsverdriet, J. W. *Surf. Sci.* **1990**, *233*, 355.

(33) Redhead, P. A. *Vacuum* **1962**, *12*, 203.

(34) Rodriguez, J. A.; Perez, M.; Jirsak, T.; Gonzalez, L.; Maiti, A. *Surf. Sci.* **2001**, *477*, L279.

(35) Sun, Y.-M.; Sloan, D.; Alberas, D. J.; Kovar, M.; Sun, Z.-J.; White, J. M. *Surf. Sci.* **1994**, *319*, 34.

(36) Rodriguez, J. A.; Jirsak, T.; Chaturvedi, S. *J. Chem. Phys.* **1999**, *111*, 8077.

(37) Raza, H.; Harte, S. P.; Muryn, C. A.; Wincott, P. L.; Thornton, G.; Casanova, R.; Rodriguez, A. *Surf. Sci.* **1996**, *366*, 519.

(38) Allen, G. C.; Tucker, P. M.; Tyler, J. W. *J. Phys. Chem.* **1982**, *86*, 224.

(39) Allen, G. C.; Tucker, P. M. *Chem. Phys. Lett.* **1976**, *43*, 254.

(40) Winer, K.; Colmenares, C. A.; Smith, R. L.; Wooten, F. *Surf. Sci.* **1987**, *183*, 67.

(41) Kotani, A.; Ogasawara, H. *Physica B* **1993**, *186−188*, 16.

(42) Winter, P. W. *J. Nucl. Mater.* **1989**, *161*, 38.

(43) Van den Berghe, S.; Miserque, F.; Gouder, T.; Gaudreau, B.; Verwerft, M. *J. Nucl. Mater.* **2001**, *294*, 168.

(44) Miserque, F.; Gouder, T.; Wegen, D. H.; Bottomley, P. D. W. *J. Nucl. Mater.* **2001**, *298*, 280.

(45) Campbell, C. T. *Surf. Sci. Rep.* **1997**, *27*, 1.

(46) Diebold, U.; Pan, J.-M.; Madey, T. E. *Surf. Sci.* **1995**, *331−333*, 845.

(47) Yakshinskiy, B. V.; Madey, T. E.; Ageev, V. N. *Surf. Rev. Lett.* **2000**, *7*, 75.

(48) Pacchioni, G.; Sousa, C.; Illas, F.; Parmigiani, F.; Bagus, P. S. *Phys. Rev. B* **1993**, *48*, 11573.

(49) Bagus, P. S.; Pacchioni, G.; Sousa, C.; Minerva, T.; Parmigiani, F. *Chem. Phys. Lett.* **1992**, *196*, 641.

(50) Sasaki, M.; Scanlon, P. J.; Ermolov, S.; Brongersma, H. H. *Nucl. Instrum. Methods Phys. Res., Sect. B* **2002**, *190*, 127.

(51) Moulder, J. F.; Stickle, W. F.; Sobol, P. E.; Bomben, K. D. *Handbook of X-ray photoelectron spectroscopy*; Perkin-Elmer Corp.: Eden Prairie, MN, 1992.

(52) Warburton, D. R.; Purdie, D.; Muryn, C. A.; Prabhakaran, K.; Wincott, P. L.; Thornton, G. *Surf. Sci.* **1992**, *269−270*, 305.

(53) Kurtz, R. L.; Henrich, V. E. *Phys. Rev. B* **1987**, *36*, 3413.

(54) Baer, Y.; Schoenes, J. *Solid State Commun.* **1980**, *33*, 885.

(55) Martin, W. C.; Musgrove, A.; Kotochigova, S.; Sansonetti, J. E. National Institute of Standards and Technology; available at: http://physics.nist.gov/PhysRefData/IonEnergy/ionEnergy.html, 2003 (Aug 17, 2004).

(56) *Handbook of Chemistry and Physics*; Lide, D. R., Ed.; CRC Press: Boston, MA, 1991.

(57) Zangwill, A. *Physics at surfaces*; Cambridge University Press: Cambridge, U.K., 1988.

(58) Hofmann, S. *Rep. Prog. Phys.* **1998**, *61*, 827.

(59) Vericat, C.; Vela, M. E.; Andreasen, G.; Salvarezza, R. C.; Vazquez, L.; Martin-Gago, J. A. *Langmuir* **2001**, *17*, 4919.

(60) Hrbek, J.; Li, S. Y.; Rodriguez, J. A.; van Campen, D. G.; Huang, H. H.; Xu, G.-Q. *Chem. Phys. Lett.* **1997**, *267*, 65.

(61) Henrich, V. E.; Cox, P. A. *The surface science of metal oxides*; Cambridge University Press: Cambridge, U.K., 1994.

(62) Lagarde, P.; Flank, A.-M.; Prado, R. J.; Bourgeois, S.; Jupille, J. *Surf. Sci.* **2004**, *553*, 115.

(63) Snyder, J. A.; Jaffe, J. E.; Lin, Z.; Hess, A. C.; Gutowski, M. *Surf. Sci.* **2000**, *445*, 495.

(64) Chaturvedi, S.; Rodriguez, J. A.; Jirsak, T.; Hrbek, J. *J. Phys. Chem. B* **1998**, *102*, 7033.

(65) Rodriguez, J. A.; Jirsak, T.; Chaturvedi, S.; Hrbek, J. *J. Am. Chem. Soc.* **1998**, *120*, 11149.

(66) Madey, T. E.; Yakshinskiy, B. V.; Ageev, V. N.; Johnson, R. E. *J. Geophys. Res.* **1998**, *103*, 5873.